UDC 54-116:54.03 **DOI: 10.15407/zht2021.67.098**

ALHASSAN ADEKU SALLAU [1,2], UMAR FARUQ HASSAN [2], ALHAJI MODU KOLO [2], ALIYU JAURO [3], ENO OKON EKANEM [4]

EFFECT OF CARBONIZATION TEMPERATURE ON PROPERTIES OF CHAR FROM CANARIUM SCHWEINFHURTHII (ATILI) SEEDSHELL

The effect of carbonization temperature on canarium schweinfhurthii seed shell was investigated. Atili seed shell particles was carbonized at different temperatures of 600, 800, 1000 and 1150°C under inert condition for 60 minutes each to obtain char products. The effect of temperature on the properties of char was investigated in detail, using several characterization techniques including, mass yield, elemental analysis, and electrical property measurements while structural transformations were monitored using X-ray diffraction, Fourier transform infrared (FTIR) spectroscopy and scanning electron microscope (SEM) techniques. The char yield decreased from 30.50 % to 26.55 % as the temperature increases from 600°C to 1150°C. The fixed carbon (82.3 to 92.66 %) and ash content (1.35 to 1.72 %) increase as temperature increase while the volatile matter (12.61 to 4.18 %) and moisture content (3.81 to 1.44 %) decreases. Ultimate analysis showed elemental carbon to increase from 85.96 % to 95.79 %. The electrical conductivity of obtained char improved significantly (1.99 x 10^{-9} to 7.24 x 10^{-2} S/cm) as well as the structural, morphology and near graphitization of char. Statistical analysis of the FTIR and XRD data via the principal component analysis showed similarity trend on the effect of temperature on the carbonization products. The improved electrical property, pore development in char morphology as well as the development of near graphitization features suggest possible use as electrode materials.

Keywords: *carbonization, correlation, conductivity, morphology, stacking.*

Досліджено вплив температури карбонізації на оболонку насіння canarium schweinfhurthii. Частинки оболонки насіння атілі карбонізували при різних температурах 600, 800, 1000 і 1150°C в інертних умовах протягом 60 хвилин для кожної з отриманням продуктів обвуглювання. Вплив температури на властивості вугілля було детально досліджено з використанням кількох методів визначення характеристик, включаючи масовий вихід, елементний аналіз та вимірювання електричних властивостей, тоді як структурні перетворення контролювали за допомогою рентгенівської дифракції, інфрачервоної спектроскопії з перетворенням Фур'є (FTIR) та скануванням методом електронної мікроскопії (SEM). При підвищенні температури від 600 °C до 1150 °C вихід вугілля зменшився з 30,50 % до 26,55 %, вміст зв'язаного вуглецю збільшується від 82,3 до 92,66 %, вміст золи збільшився від 1,35 до 1,72 %, тоді як зменшується вміст летких речовин (від 12,61 до 4,18 %) і вміст вологи (від 3,81 до 1,44 %). Остаточний аналіз показав, що вміст елементного вуглецю збільшився з 85,96 % до 95,79 %. Електропровідність отриманого вугілля значно покращилася (від 1,99 x 10^{-9} до 7,24 x 10^{-2} S/cm), а також структура, морфологія майже графітизованого вугілля. Статистичний аналіз даних FTIR та XRD через аналіз головних компонентів показав подібну тенденцію щодо впливу температури на продукти карбонізації. Поліпшені електричні властивості, розвиток пор у морфології вугілля, а також розвиток ознак, близьких до графітизації, передбачають можливе використання продуктів карбонізації як електродних матеріалів.

Ключові слова: *карбонізація, кореляція, провідність, морфологія, стекінг.*

Исследовано влияние температуры карбонизации на оболочку семян canarium schweinfhurthii. Частицы скорлупы семян атили карбонизировали при различных

температурах 600, 800, 1000 и 1150°C в инертных условиях в течение 60 мин каждая для получения полукоксовых продуктов. Влияние температуры на свойства полукокса было подробно исследовано с использованием нескольких методов характеризации, включая массовый выход, элементный анализ и измерения электрических свойств, в то время как структурные превращения контролировались с помощью рентгеновской дифракции, инфракрасной спектроскопии с преобразованием Фурье (FTIR) и сканирования методом электронной микроскопии (SEM). Выход полукокса снижался с 30,50 % до 26,55 % при повышении температуры от 600°C до 1150°C. Связанный углерод (от 82,3 до 92,66 %) и содержание золы (от 1,35 до 1,72 %) увеличиваются с повышением температуры, тогда как содержание летучих веществ (от 12,61 до 4,18 %) и содержание влаги (от 3,81 до 1,44 %) уменьшаются. Окончательный анализ показал, что содержание элементного углерода увеличилось с 85,96 % до 95,79 %. Электропроводность полученного угля значительно улучшилась (с $1{,}99\times10^{-9}$ до $7{,}24\times10^{-2}$ S/cm), а также структура, морфология и почти графитизированного угля. Статистический анализ данных FTIR и XRD с помощью анализа основных компонентов показал сходную тенденцию влияния температуры на продукты карбонизации. Улучшенные электрические свойства, развитие пор в морфологии полукокса, а также развитие признаков, близких к графитизации, предполагают возможное использование продуктов карбонизации в качестве электродных материалов.

***Ключевые слова**: карбонизация, корреляция, проводимость, морфология, стэкинг.*

Introduction

Canarium schweinfurthii bursaraceae is a Nigerian perennial tree with a fruit called atili in Hausa and Okpoko in Ibo [1]. The plant is a massive forest tree with a crown that reaches the forest's high canopy and a 50-meter-long clean, straight, and cylindrical bole [2]. From Senegal through west Cameroon and on to Ethiopia, Tanzania, and Angola, Atili may be found in tropical Africa's rain forest, gallery forest, and transitional forest [2-3]. The fruit is composed comprised of a seed and a delicious pulp. The shell and germ combine to form the seed, which is a tough mass. Oils can be present in the pulp as well as in the germ. The pulp is commonly eaten raw, cooked, or used as a spice. The pulp oil has more saturated fatty acids, whereas the germ (kernel) oil has more unsaturated fatty acids and is less sticky. The nutritional value of Atili pulp and germ has been studied by a number of writers. Nyam et al. [4] determined the proximate, anti-nutrient, and elemental content of a variety of atili fruits. The crude fat level of fruit pulp was 64.04 %, the protein content was 6.39 %, the fiber content was 16.37 %, and the carbohydrate content was 3.85 %, according to their data. Anti-nutrient values of 240 mg/100 g, 162 mg/100 g, and 26 mg/100 g were observed for tannins, phytic acid, and oxalate, respectively. Olawale reported on the physical, chemical, and technical properties of the Atili fruit's pulp and kernel oils, as well as their prospective industrial uses [3]. The pulp oil contains around 70% palmitic acid, has a specific gravity of 0.937, a specific heat capacity of 3999.50 J/g°C, and calorific values of 42.32 MJ/kg, according to the article. The kernel oil had a specific gravity of 0.910, a specific heat capacity of 3837.54 J/g°C, and calorific values of 36.488 MJ/kg, and it included roughly 26% palmitic acid and more than 64% oleic/linoleic acids. The synthesis of activated carbon from Atili's nutshell for use in adsorption tests has been the subject of several studies [5-11]. As a result, the goal of this study is to investigate how temperature treatment affects the proximal, ultimate, structural, and electrical properties of atili seed shell char (ASS).

Experimental

Atili fruits were purchased in Jos, Plateau State, Nigeria's. To isolate the germ from the shells, the pulp was removed and the nut was cracked. After air drying for 48 hours, the shells were

crushed and sieved with a 2mm sieve. These were then packed into a 410mm stainless-steel combustion tube (34.5mm inner and 42.5mm outer diameter) and placed in a thermolyte tubular furnace for 60 minutes at temperatures of 600°C, 800°C, 1000°C, and 1150°C in a nitrogen gas atmosphere. The proximate analysis of the Atili seed shell and char products was performed using standard American Society for Testing and Materials (ASTM) methodologies D 4442 – 07 and D1762-84, respectively. At the Umar Musa Yar'adua University's central laboratory in Katsina, Nigeria, the ultimate analysis was done using a Perkin Elmer 2400 Series II CHN Elemental Analyzer, and the morphological structure was evaluated using a Phenom ProX scanning electron microscope. The Chemistry Advanced Research Center, Sheda Science and Technology Complex (SHESTCO), Abuja, Nigeria, employed a Thermo Scientific Nicolet iS5 FT-IR Spectrometer to investigate functional groups. The crystal structure was determined at the National Geological Research Laboratory in Kaduna, Nigeria, using an empyrean (panalytical) diffractometer. At the Physics Advanced Research Center, SHESTCO, Abuja, Nigeria, the electrical characteristics were examined using a four-point probe linked to a Keithley source meter for voltage, current sourcing, and lab-tracer 2.0 software.

Result and discussions

Proximate analysis and ultimate analysis: The ASS raw had a high volatile matter of 73.33 %, a fixed carbon of 19.03 %, an ash content of 1.11 %, and a moisture of 6.53 %, according to the proximate analysis (Table 1). As the temperature rose from 600 to 1150 °C, the yield of ASS char decreased from 29.69 % to 25.27 %. This is most likely owing to the atili seed shell losing more volatile components as the temperature increased [8]. Moisture and volatile matter content in char formed at different temperatures decreased with increasing temperature, but fixed carbon and ash content rose. As can be shown, char with higher carbonization temperatures has a higher fixed carbon content than char with lower carbonization temperatures. Meanwhile, with increasing temperature treatment, the volatile matter content of the generated char was shown to decrease. This might indicate that char produced at higher temperatures is more stable than char produced at lower temperatures [12]. Similarly, the percentage carbon increased significantly in all of the char formed at various temperatures, according to the elemental composition data. ASS 600, for example, had a 75 percent increase, whereas ASS 1150 saw a 200 percent increase.

Electrical resistance and conductivity

The electrical conductivity of ASS char increased from 1.99 x 10^{-9} S/cm at 600 °C to 7.24 x 10^{-2} S/cm at 1150 °C. Electrical conductivity in carbon materials has been discovered to be influenced by compression force [13-15], crystallinity, activation, and the presence of pores. As a consequence, higher carbonization temperatures resulted in more conductive phase in the carbonized ASS, most likely due to more carbon atoms being integrated into the disordered graphene sheets often associated with charcoal [17].

Table 1

Proximate and ultimate analysis carbon material and char products

		Proximate Analysis				Ultimate Analysis					Conductivity
	Yield	MC	VM	FC	Ash	C	H	O	N	S	S/cm
ASS Raw		**6.53**	**73.33**	**19.03**	**1.11**	**49.03**	**5.01**	**44.75**	**1.19**	**0.02**	
ASS600	**30.59**	**3.81**	**12.61**	**82.23**	**1.35**	**85.96**	**4.17**	**9.31**	**0.55**	**0.01**	**1.99×10^{-9}**
ASS800	**27.03**	**2.53**	**9.27**	**86.78**	**1.42**	**89.97**	**3.01**	**6.74**	**0.27**	**0.01**	**9.04×10^{-3}**
ASS1000	**27.91**	**1.82**	**5.88**	**90.67**	**1.63**	**92.69**	**2.61**	**4.57**	**0.12**	**0.01**	**2.20×10^{-2}**
ASS1150	**26.55**	**1.44**	**4.18**	**92.66**	**1.72**	**95.79**	**1.04**	**3.05**	**0.11**	**0.01**	**7.24×10^{-2}**

MC-moisture content, VM-volatile matter, FC-fixed carbon

Functional Group Investigation by FTIR

The IR spectra of the ASS raw and char products at various carbonization temperatures are shown in Figure 1. The O-H group, which is considered to be made up of water, alkanols, or carboxylic acid, was attributed to the wide band peak at 3345 cm^{-1} seen in the ASS raw sample. In char samples, the peak faded, indicating that it was generated by water (moisture).

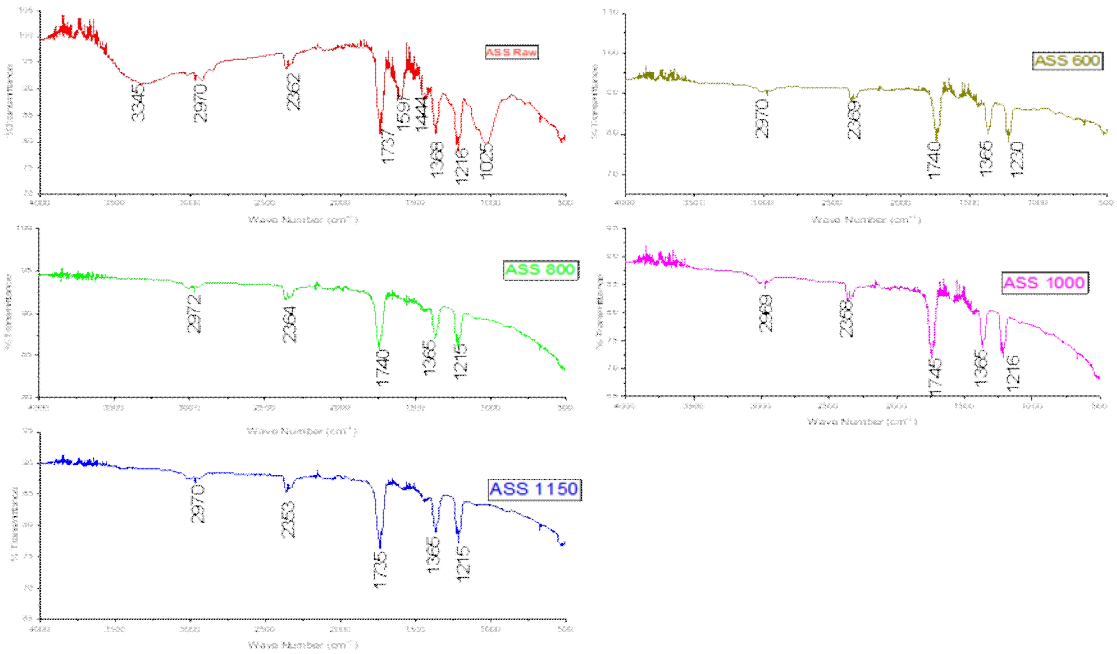

Figure 1. FTIR spectra of ASS and its chars obtained at different temperatures.

C=O was ascribed to the high signal at 1737 cm^{-1}, perhaps due to unconjugated uronic anhydride, whereas C-O stretching in the C-O-H of the phenolic group was attributed to the medium peak at 1218 cm^{-1} [18]. A methyl C-H asymmetric stretch [19] was allocated to the weak peaks at 2970 cm^{-1}, whereas an alkyne C=C stretch was assigned to the weak peaks at 2362 cm^{-1} [20]. The medium stretch peaks at 1368 cm^{-1} were attributed to symmetric N-O stretching of aliphatic nitro-compounds, which is frequently observed between 1380-1350 cm^{-1} [21], as well as the O-H group, which can be seen between 1395 cm^{-1} and 1360 cm^{-1} as a sign of the presence of various alcohols and phenols [22]. C=C-C of aromatic ring [23] is represented by the medium peak stretch at 1597 cm^{-1}. The stretching mode of vibration of C–O of cellulose, hemicelluloses, and lignin induced the peak at 1040.62 cm^{-1} [24-25]. Unconjugated C=O had the greatest absorption band at 1736.94 cm^{-1}, medium stretch at 1365.43 cm^{-1} for aliphatic nitro compounds, and medium stretch at 1216.79 cm^{-1} for C-O stretching in the ASS char samples. Additional very weak peaks were found at 2969.92 cm^{-1} for a methyl C-H asymmetric stretch and 2359.92 cm^{-1} for an alkyne C=C stretch. The intensity of these peaks diminished as the carbonization temperature rose. Principal component analysis (PCA) was used on the spectra data to look for any changes in the structure of the char samples as the temperature changed. PCA has been suggested as a useful strategy for minimizing variables [24,26]. In PCA analysis, samples that seem near to one another indicate similarity, while samples that appear far away indicate differences. This type of analysis provides considerable difference between samples as an identification tool [27].

Table 2

Correlation for the sample spectra data

	ASS raw	ASS600	ASS800	ASS1000	ASS1150
ASS raw	1	0.92702	0.91456	0.9211	0.8912
ASS600	0.92702	1	0.99183	0.99051	0.9649
ASS800	0.91456	0.99183	1	0.97239	0.9276
ASS1000	0.9211	0.99051	0.97239	1	0.98639
ASS1150	0.8912	0.9649	0.9276	0.98639	1

The five samples were strongly correlated, as shown in Table 2, with correlation coefficient values greater than 0.5, indicating that PCA was an appropriate method for analyzing the data. The Eigenvalues of the Correlation Matrix, as shown in Table 3, revealed that the first principle component explained 95.93 % of the variance, while the second principal component contributed only 2.50 % and the remaining components each contributed less than 2%. Furthermore, the PC loading plot in Figure 2 revealed that the ASS raw differs significantly from the char products, which are stacked perpendicularly.

Table 3

Eigenvalues of the Correlation Matrix

	Eigenvalue	Percentage of Variance	Cumulative
1	4.79639	95.93 %	95.93 %
2	0.12504	2.50 %	98.43 %
3	0.07459	1.49 %	99.92 %
4	0.00354	0.07 %	99.99 %
5	4.36E-4	0.01 %	100.00 %

Despite the fact that in both the ASS raw and ASS char samples, only PC 1 accounted for the bulk of variation. This suggests that adjusting the carbonization temperature can result in significant differences in the structural features of the char generated [28].

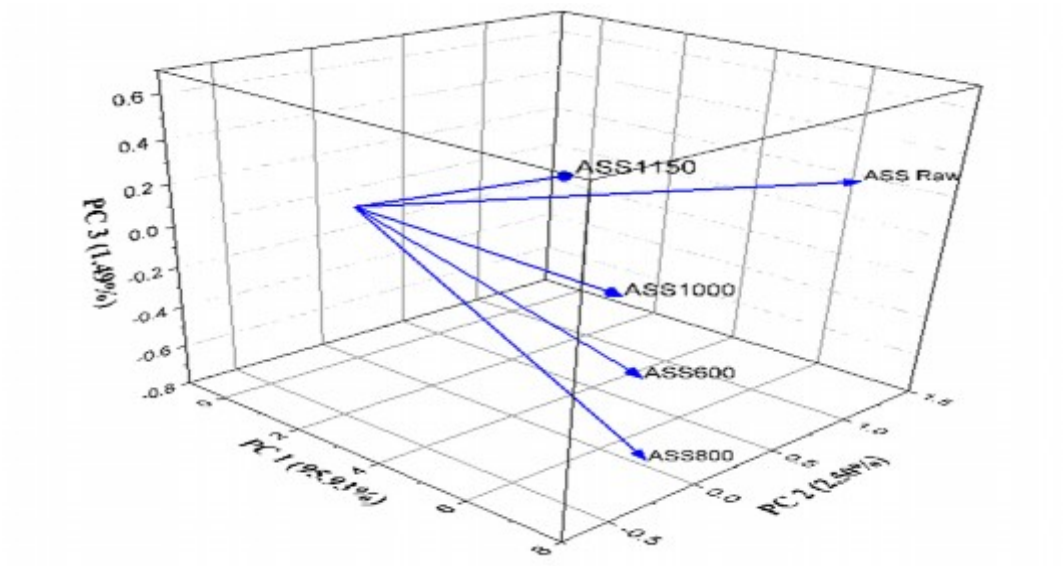

Figure 2. PCA of FTIR data for the ASS raw and four char obtained at different temperatures.

XRD Analysis

The XRD spectra of ASS raw and char at various carbonization temperatures are shown in Figure 3. The diffractograms appeared to display similar peaks (002) between 20-25, 2 theta angle and peak (100) between 42-47, 2 theta angle when the treatment temperature rose. The stacking of char crystallite graphitic basal plans is often associated with these peaks [29]. According to XRD theory, asymmetric XRD peaks can be recognized when a sample has a stacked crystal structure or the sample composition is not uniform. A carbon material with a graphite structure displays asymmetry of the (002) peak due to stacking defects [30].

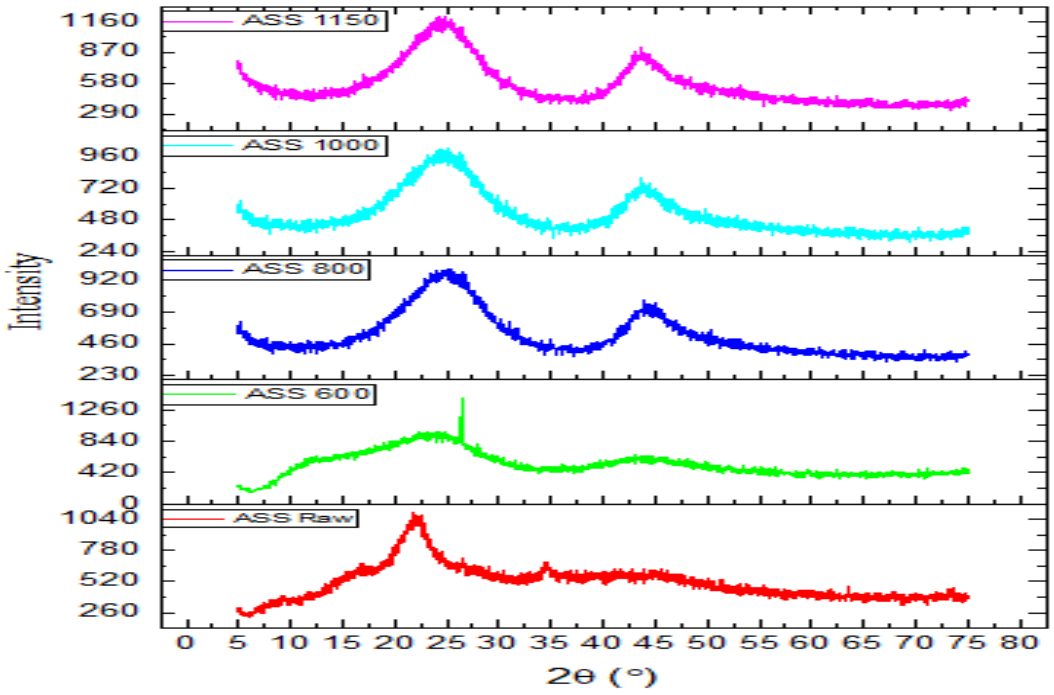

Figure 3. X-ray diffraction for ASS raw and char samples at various temperature.

Crystallite geometry in carbon materials parameters such as aromatic layer stacking height (Lc), diameter (La) and inter-layer spacing (d_{002}) was estimated using the Bragg's law and Scherrer equation [31,32].

$$d = \frac{\lambda}{2sin\theta(002)} \quad (1)$$

$$L_c = \frac{0.94\lambda}{\beta(002)cos\theta(002)} \quad (2)$$

$$L_a = \frac{1.84\lambda}{\beta_{100}\cos(\theta_{100})} \quad (3)$$

$$n\lambda = 2d_{002}\sin(\theta_{002}) \quad , \quad (4)$$

where λ is the wavelength of the X-ray radiation (1.540598), $d_{(002)}$ is the width of the (002) peak at half maximum of reflection, and θ is the Bragg peak position.

Table 4 shows that when the carbonization temperature rises, the value of d (002) decreases from 4.0219 in raw ASS to 3.6320 in ASS 1150, whereas d (100) grows fractionally from 2.0680 in ASS 600 to 2.0726 in ASS 1150, despite being nonexistent in raw ASS.

Table 4

Structure parameters of XRD for ASS raw and char samples at various temperature

Sample	d_{002} (A°)	d_{100}(A°)	L_c (A°)	L_c/d_{002}	Ac	DOC
ASS Raw	4.0219	-	0.004839	0.001203	92.38	7.62
ASS 600	3.7473	2.0680	1.123164	0.299726	94.72	5.28
ASS 800	3.6147	2.0709	0.052066	0.014420	93.09	6.91
ASS 1000	3.6389	2.0783	0.053078	0.014753	91.46	8.54
ASS 1150	3.6320	2.0726	0.057103	0.015822	91.27	8.73

Ac – Amorphous content, DOC – Degree of crystallinity

The numerical variance of d (002) was found to be greater than that of d (100), which matches the results of typical carbon materials [33-34]. The tiny peak at roughly 26-27 2theta also disappeared when the carbonization temperature rose. In addition, when the temperature rises from 600 to 1150 ℃, the char's crystallinity increases. However, because these equations are derived for highly graphitized carbons and are not suitable for entirely disordered carbons, computed Lc and La values are not precisely equal to the stacking height and lateral dimension of the crystallites. As a result, they may be used to calculate the real stacking height and lateral dimension of crystallites [31]. As a result, real crystallite sizes will almost certainly be greater than expected. PCA was used on the data from the XRD diffractograms to find similarities and differences in the ASS char samples gathered. With all values more than + 0.5, the sample data was shown to be substantially linked. Table 5 shows the details of the linear correlation strength between the ASS raw and char samples.

Table 5

Correlation of XRD Data

	ASS raw	ASS600	ASS800	ASS1000	ASS1150
ASS raw	1	0.85647	0.72637	0.73764	0.70086
ASS600	0.85647	1	0.81359	0.81916	0.78604
ASS800	0.72637	0.81359	1	0.97853	0.97579
ASS1000	0.73764	0.81916	0.97853	1	0.97586
ASS1150	0.70086	0.78604	0.97579	0.97586	1

As indicated by a correlation value of 0.975, the ASS 1150 char sample had the highest linear relation with ASS 1000 and ASS 800. The first main component accounts for 87.13 % of the variance, whereas the second component accounts for 9.37 %, according to the Eigenvalues of the Correlation Matrix, as shown in Table 6. The remaining 3% of the overall variance is contributed by each of the others. In contrast, the PC loading plot in Figure 4 revealed the ASS raw and ASS 600 as two groups with comparable variance and distinct from the ASS 800, ASS 1000, and ASS 1150 groups.

Table 6

Eigenvalue of Correlation Matrix of Sample PCA

	Eigenvalue	Percentage of Variance	Cumulative
1	4.35672	87.13 %	87.13 %
2	0.46864	9.37 %	96.51 %
3	0.13021	2.60 %	99.11 %
4	0.02321	0.46 %	99.58 %
5	0.02122	0.42 %	100.00 %

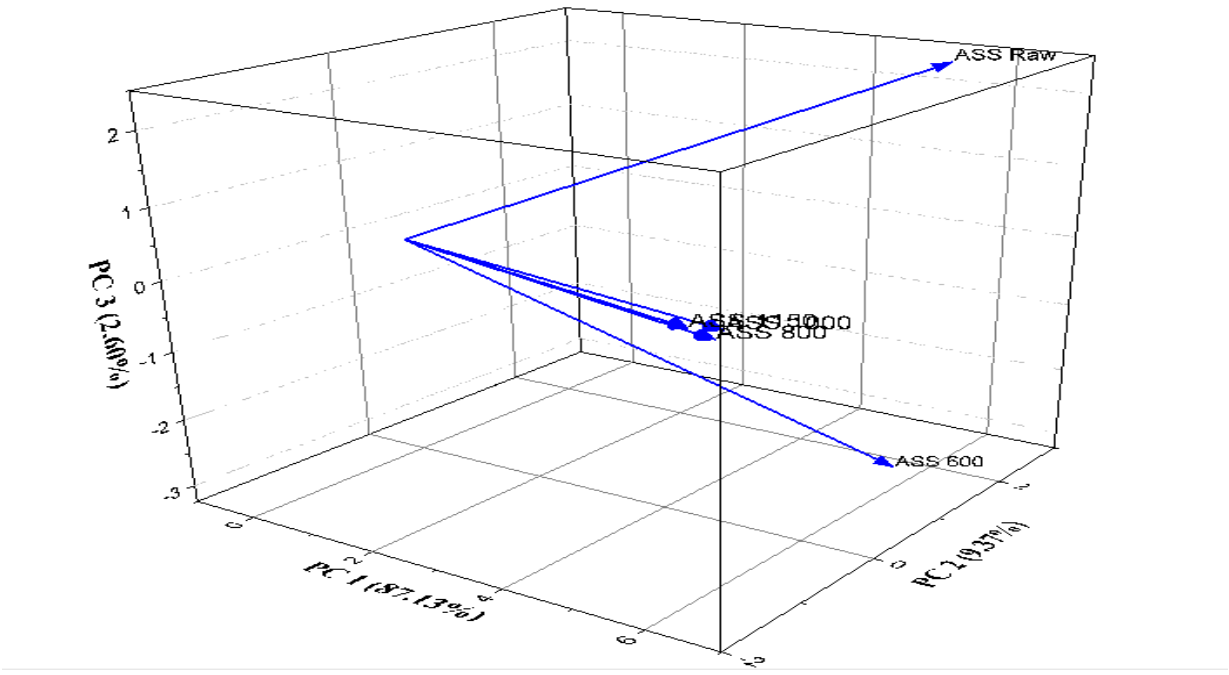

Figure 5. PCA loading plot of all samples.

SEM Analysis

SEM images of Atili seed shell powder and Atili seed shell char generated at temperatures of 600, 800, 1000 and 1150 °C for external morphology are shown in Figure 6. The raw atili shell displayed a fibrous structure with a few holes ranging in size from 2.42 to 10.41m at 2000x magnification. As the carbonization temperature rises, the chars' surface shape changes dramatically. Bubbles and holes formed as a result of the discharge of volatiles. In the range of 2.63 to 8.51 m, the ASS 600's surface features few holes.

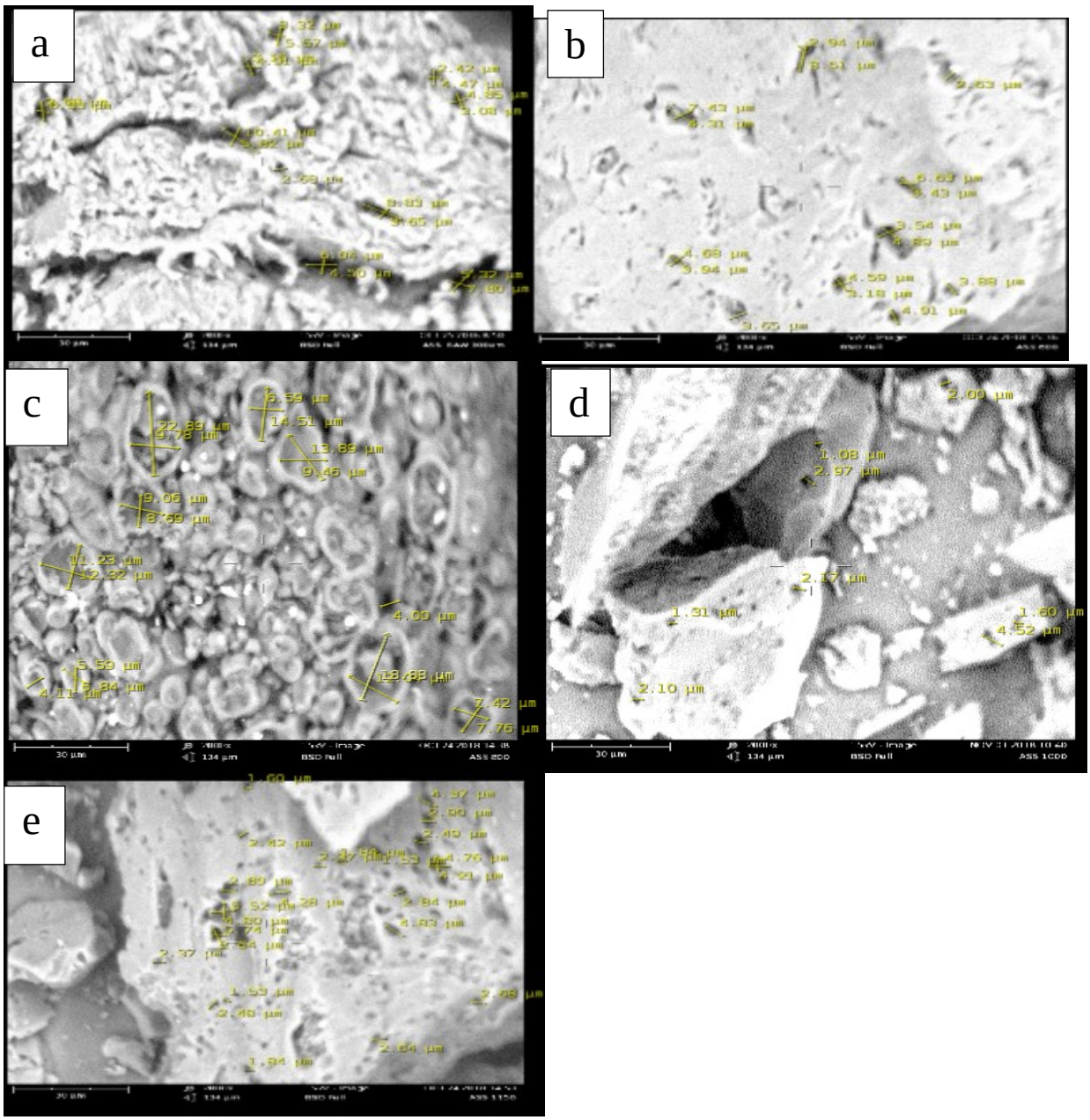

Figure 6. SEM image (a) ASS Raw (b) ASS 600 (c) ASS 800 (d) ASS 1000 (e) ASS 1150.

On the surface of ASS 800 char, additional heart-shaped opened fissures with diameters ranging from 4.00 to 22.89 m were evident. Surprisingly, compared to ASS 800 char, the surface of ASS 1000 exhibited less visible pores; this might be due to the SE microgram's viewpoint. More pores with diameters ranging from 1.60 to 5.74 m were observed on the ASS 1150. This might indicate that raising the temperature caused pores to form on the surface in general.

Conclusion

The char characteristics were shown to be significantly influenced by the carbonization temperature. While the lone aromatic carbon structure was detected to disappear in the IR spectra as the temperature rose, the electrical conductivity of char increased, additional pores grew on the char surface, and other polar and pi bond groups were conserved.

Acknowledgements

Dr. Abayomi T. O., Dr. Stella A. E., Mr David B. M. of Chemistry Advanced Research Center, and Dr. Thomas Imeleria at Physics Advance Research Center, SHESTCO, Abuja, Nigeria deserve special thanks for their help and patience.

REFERENCES

1. ***Agu H.O., Ukonze J.A. Uchola N.O.*** Quality and characteristics of crude and refined Atili Oils. *Pakistan journal of nutrition.* 2008. 7(1). P. 27-30.

2. ***Maina S.N. Anuka A.A.*** Production of activated carbon from Atili seed shells. *Leonardo Electronic Journal of Practices and Technologies.* 2014. 25. P. 195-209.

3. ***Olawale S.A.*** Industrial Properties of Oils of African Elemi (*Canarium schweinfurthii*) Fruit. *JOMAR.* 2014. 8(1 & 2). P. 42-49.

4. ***Iretiola J.P.*** Production of Activated Carbon from shell of *Canarium schweinfurthii* seed. 2001. A B. Eng. Research Project Report, Chemical Engineering Department, Ahmadu Bello University, Zaria. Nigeria.

5. ***Olawale A.S., Ajayi A.O. Jegede I.P.*** Development of Activated Carbon from *Canarium schweinfhurthii* nutshell: A Preliminary Study. A paper presented at the 41st Annual Conference of Science Association of Nigeria held at Usmanu Danfodiyo University, Sokoto, Nigeria. 2005. 25th-29th April.

6. ***Yilleng, M.T., Gimba C.E., Ndukwe, I.G. Nwankwere, E.T.*** Adsorption of hexavalent chromium from aqueous solution by granulated activated carbon from *Canarium schweinfurthii* seed shell. *Advances in Applied Science Research.* 2013. 4(3) P. 89-94.

7. ***Abugu H.O., Okoye P.A.C., Ajiwe V.I.E. Ofordile P.C.*** Preparation and Characterization of Activated Carbon from Agro wastes Peanut Seed (African Canarium) and Palm *Kernel* Shell. *International journal of innovative research & development.* 2014. 3(13). P. 418-441.

8. ***Yilleng M.T., Bahago N., Gojeh M., Wyasu G. Emmanuel C.G.*** Adsorption of Dichlorvos in aqueous solution onto Activated Carbon from Canarium Schweinfurthii Seed Shell. *International Journal of Scientific & Engineering Research.* 2016. 7(2). P. 2229-5518. http://www.ijser.org

9. ***Maguie K., Nsami N., Daouda K., Randy C., Mbadcam K.*** Adsorption Study of the Removal of Copper (II) Ions using Activated Carbon Based CanariumSchweinfurthii Shells Impregnated with $ZnCl_2$. *IRA International Journal of Applied Sciences.* 2017. 8(1), P. 18-30. DOI: http://dx.doi.org/10.21013/jas.v8.n1.p2

10. ***Zaharaddeen N.G., Hussin H.M., Galadima A. Lawan I.*** Potentials of *Canarium schweinfurthii*seed shell as a novel precursor for CH_3COOK activated carbon: statistical optimization, equilibrium and kinetic studies. *Applied Water Science.* 2019. 9. 31. https://doi.org/10.1007/s13201-019-0907-y.

11. ***Lee L.C., H'ng S.P., Paridah T., Chin L.K., Khoo S.P., Nazrin R.A.R., Asyikin N.S., Maminski M.*** Effect of Reaction Time and Temperature on the Properties of Carbon Black Made from Palm Kernel and Coconut Shell. *Asian journal of scientific research.* 2017. 10 (10). P. 24-33.

12. ***Liyanage D. C., Pieris M.*** A physico-chemical analysis of coconut shell powder. *Procedia chemistry*. 2015. 16. P. 222-228. www.sciencedirect.com.

13. ***Coates J.*** Interpretation of Infrared Spectra, A Practical Approach, Encyclopedia of Analytical Chemistry. Copyrights John Wiley & Sons Ltd. 2019. P. 1-23. http://www3.uma.pt/jrodrigues/disciplinas/QINO-II/Teorica/IR.pdf.

14. ***Okolo I.B., Oke O.E., Agu M.C., Adeyi O., Nwoso‑Obieogu K., Akatobi N.K.*** Adsorption of Lead(II) from Aqueous Solution using Africa Elemi Seed, MucunaShell and Oyster Shell as Adsorbents and Optimization using Box–Behnken Design. *Applied Water Science*. 2020. 10:201. https://doi.org/10.1007/s13201-020-01242-y

15. ***Nandiyanto A.B.D., Oktiani R. and Ragadhita R.*** How to Read and Interpret FTIR Spectroscope of Organic Material. *Indonesian Journal of Science & Technology*. 2019, 4(1). P 97-118.

16. ***Yahaya Z.A., Somalua R.M., Muchtara A., Sulaimanc A.S., Daud W.R.W.*** Effects of temperature on the chemical composition of tars produced from the gasification of coconut and palm kernel shells using downdraft fixed-bed reactor. *Fuel*. 2020. 265. Article 116910 https://doi.org/10.1016/j.fuel.2019.116910

17. ***Liu Y., He Z, Uchimiya M.*** Comparison of Biochar Formation from Various Agricultural By-Products Using FTIR Spectroscopy. *Modern Applied Science.* 2015. 9(4). P 246-253. www.ccsenet.org/mas

18. ***Satheesh M., Pugazhvadivu M., Prabu B., Gunasegaran V. Manikandan A.*** Synthesis and Characterization of Coconut Shell Ash. *Journal of Nanoscience and Nanotechnology*. 2019. 19. P. 4123-4128. www.aspbs.com/jnn

19. ***Sanguansat P. (ed.).*** Principal component analysis – engineering applications. Intech, 2012. Rijeka, Croatia.

20. ***Noh C.H.C., Azmin N.F.M., Amid A.*** Principal Component Analysis Application on Flavonoids Characterization. *Advances in Science, Technology and Engineering Systems Journal*. 2017. (2) 3. P. 435-440.

21. ***Reeves J.*** Mid-Infrared Spectroscopy of Biochars and Spectral Similarities to Coal and Kerogens: What are the Implications? *Appl. Spectr.* 2012. 66. P. 689-695. http://dx.doi.org/10.1366/11-06478

22. ***Wang P., Zhang J., Shao O., Wang G.*** Physicochemical properties evolution of chars from palm kernel shell pyrolysis. *Journal of Thermal Analysis and Calorimetry*. 2018. https://doi.org/10.1007/s10973-018-7185-z(0123456789.

23. ***Kang S.D., Lee M.S., Lee H.S. Roh S.J.*** X-ray diffraction analysis of the crystallinity of phenolic resin-derived carbon as a function of the heating rate during the carbonization process. *Carbon Letters.* 2018. 27, P. 108-111. DOI: https://doi.org/10.5714/CL.2018.27.108

24. ***Girgis S.B., Temerk M.Y., Gadelrab M.M. Abdullah D.I.*** X-ray Diffraction Patterns of Activated Carbons Prepared under Various Conditions. *Carbon science.* 2007. 8(2). P. 95-100. DOI https://doi.org/10.5714/CL.2007.8.2.095

25. ***Stein I.Y., Ashley L.K., Alexander J.C., Luiz A. Brian L.W.*** Mesoscale Evolution of Non-Graphitizing Pyrolytic Carbon in Aligned Carbon Nanotube Carbon Matrix Nanocomposites. *Journal of Materials Science.* 2017. 52(24). P. 13799-13811.

26. ***Ma X., Yuan C. and Liu X.*** Mechanical, Microstructure and Surface Characterizations of carbon Fibers Prepared from Cellulose after Liquefying and Curing. *Materials.* 2014. 7. P. 75-84; DOI:10.3390/ma7010075

27. ***Barnakov N.C., Khokhlova P.G., Malysheva Y.V., Popova N.A. and Ismagilov R.Z.*** X–Ray Diffraction Analysis of the Crystal Structures of Different Graphites. *Solid Fuel Chemistry.* 2015. 49(1), P. 25–29.

[1]*Chemistry Advanced Research Center,Sheda Science and Technology Complex, Abuja*

[2]*Department of Chemistry, Abubakar Tafawa Balewa University Bauchi, Bauchi State*

[3]*National Environmental Standards and Regulations Enforcement Agency (NESREA), Abuja*

[4]*Department of Chemistry, Federal University Otuoke, Bayelsa State*

Received on December 22, 2021